Inorganic Chemistry
Article

Inorg. Chem. **2009,** *48,* 4661–4673 **4661**
DOI:10.1021/ic900055d

Molecular-Programmed Self-Assembly of Homo- and Heterometallic Tetranuclear Coordination Compounds: Synthesis, Crystal Structures, and Magnetic Properties of Rack-Type $Cu^{II}_2M^{II}_2$ Complexes (M = Cu and Ni) with Tetranucleating Phenylenedioxamato Bridging Ligands

Emilio Pardo,[†] Danielle Cangussu,[†,◆] Rodrigue Lescouezec,[†] Yves Journaux,*[,†] Jorge Pasán,[‡] Fernando S. Delgado,[§] Catalina Ruiz-Pérez,* Rafael Ruiz-García,[∥,⊥] Joan Cano,[#,▽] Miguel Julve,[○] and Francesc Lloret*[,○]

[†]*Laboratoire de Chimie Inorganique et Matériaux Moléculaires, Université Pierre et Marie Curie-Paris 6, UMR 7071, Paris, F-75005 France,* [‡]*Laboratorio de Rayos X y Materiales Moleculares, Departamento de Física Fundamental II, Facultad de Física, Universidad de la Laguna, La Laguna, Tenerife, E-38204 Spain,* [§]*BM16-LLS European Synchrotron Radiation Facility, BP 220, Grenoble Cedex 9, 38043 France,* [∥]*Departament de Química Orgànica/Instituto de Ciencia Molecular (ICMol), and* [⊥]*Fundació General de la Universitat de València (FGUV) Universitat de València, Paterna, Valencia, E-46980 Spain,* [#]*Departament de Química Inorgànica/Institut de Química Teòrica i Computacional (IQTC),* [▽]*Institució Catalana de Recerca i Estudis Avançats (ICREA), and Universitat de Barcelona, Barcelona, E-08028 Spain, and* [○]*Departament de Química Inorgànica/Instituto de Ciencia Molecular (ICMol), Universitat de València, Paterna, Valencia, E-46980 Spain.* [◆] *Present address: Instituto de Química, Universidade Federal de Goiás, Goiânia, GO 74001-970 Brazil*

Received January 12, 2009

New homo- and heterobimetallic tetranuclear complexes of formula $[Cu_4(mpba)(Me_4en)_4(H_2O)_4](ClO_4)_4\cdot 3H_2O$ (**1**), $[Cu_4(mpba)(Me_4en)_4(H_2O)_4](PF_6)_4\cdot 2H_2O$ (**2**), $[Cu_4(ppba)(Me_4en)_4(H_2O)_4](ClO_4)_4\cdot 2H_2O$ (**3**), $[Cu_4(mpba)(dipn)_4](ClO_4)_4\cdot 3H_2O$ (**4**), $[Cu_4(ppba)(dipn)_4](ClO_4)_4\cdot 2H_2O$ (**5**), and $[Cu_2Ni_2(ppba)(dipn)_4(H_2O)_2](PF_6)_4$ (**6**) [mpba = *N*,*N*′-1,3-phenylenebis(oxamate), ppba = *N*,*N*′-1,4-phenylenebis(oxamate), Me_4en = *N*,*N*,*N*′,*N*′-tetramethylethylenediamine, and dipn = dipropylenetriamine] have been synthesized and structurally and magnetically characterized. Complexes **1**−**6** have been prepared following a molecular-programmed self-assembly method, where a heteropolytopic tetranucleating phenylenedioxamato bridging ligand (L = mpba or ppba) is bound to four metal ions of identical or different natures ($M = Cu^{II}$ and/or Ni^{II}) with partially blocked coordination sites by bi- or tridentate polyamine terminal ligands (L′ = Me_4en or dipn). The structures of **1**−**6** consist of cationic tetranuclear $Cu^{II}_2M^{II}_2$ entities with an overall ^{4}R rack-type architecture, which is made up of two oxamato-bridged homo- (**1**−**5**) or heterodinuclear (**6**) $Cu^{II}M^{II}$ units (M = Cu and Ni) connected through either a meta- (**1**, **2**, and **4**) or a para-substituted (**3**, **5**, and **6**) phenylene spacer between the Cu^{II} ions. The magnetic properties of **1**−**6** have been interpreted according to their "dimer-of-dimers" structure [$\mathbf{H} = -J(\mathbf{S}_1\cdot\mathbf{S}_2 + \mathbf{S}_3\cdot\mathbf{S}_4) - J'(\mathbf{S}_1\cdot\mathbf{S}_3)$ with $S_1 = S_3 = S_{Cu} = 1/2$ and $S_2 = S_4 = S_M = 1/2$ (M = Cu) or 1 (M = Ni)]. The homometallic Cu^{II}_4 complexes exhibit either strong ($-J = 330-350$ cm^{-1}) or weak-to-moderate ($-J = 4.8-87.1$ cm^{-1}) antiferromagnetic intradimer couplings through the oxamato bridge, depending on the bi- (**1**−**3**) or tridentate (**4** and **5**) nature of the terminal ligand, respectively. The heterometallic $Cu^{II}_2Ni^{II}_2$ complex with a tridentate terminal ligand (**6**) shows instead a moderate antiferromagnetic intradimer coupling ($-J = 50$ cm^{-1}). Otherwise, the nature and magnitude of the interdimer coupling cannot be unambiguously determined except for the pair of homo- and heterometallic $Cu^{II}_2M^{II}_2$ complexes [M = Cu (**5**) and Ni (**6**)] with the *p*-phenylenedioxamato bridging ligand and a tridentate terminal ligand, which show a weak antiferromagnetic interdimer coupling ($-J' = 14$ and 23 cm^{-1}) across the para-substituted phenylene spacer.

Introduction

Metallosupramolecular chemistry opens wide perspectives for the rational design of multimetallic coordination architectures with a seemingly limitless range of structural motifs which are based on metal−ligand coordinative interactions.[1] These include a great variety of discrete polynuclear coordination compounds formed by the molecular-programmed

* To whom correspondence should be addressed. E-mail: yves.journaux@upmc.fr (Y.J.); caruizperez@gmail.com (C.R.P.); francisco.lloret@uv.es (F.L.).

(1) (a) Lenninger, S.; Olenyuk, B.; Stang, J. *Chem. Rev.* **2000**, *100*, 853. (b) Swiegers, G. F.; Malefetse, T. J. *Chem. Rev.* **2000**, *100*, 3483.

Published on Web 3/30/2009

self-assembly of polytopic aromatic organic ligands and transition metal ions.[2−6] They display latticed (metal grids, ladders, and racks), cyclic (polygonal or polyhedral metal cages), filamentous (metal rods and metallodendrimers), or interlaced motifs (metal rotaxanes, catenanes, and knots).[1b] Some of them are formed by templation with counterions, either anions[7] or cations,[8] that are hosted within the confined space of the charged metal cage where they are held through ionic interactions or weak coordinative bonds. Others are even able to reversibly bind or stabilize neutral guest molecules through hydrophobic interactions and hydrogen bonds.[9] The presence of paramagnetic transition metal ions in these metallosupramolecular complexes may lead to new magnetic properties which result from the cooperative exchange interactions between the metal ions through the bridging ligands. This is illustrated by the research work of Thompson, Lehn, and others on the magnetic properties of self-assembling transition metal grids of varying nuclearities with pyrimidine, phenoxo, tetrazolylamido, and methoxydiazine-based bridging ligands.[5,6] Such magnetically coupled metallosupramolecular complexes can play a relevant role in the so-called "bottom-up" approach to molecular-level electronic devices with potential applications in future information storage and processing nanotechnology.[6]

In the search for magnetically coupled, homo- and heterometallic polynuclear coordination compounds with aromatic polyoxamato (APOXA) ligands,[10] we recently prepared double-stranded dinuclear copper(II) complexes of the metallacyclophane type by the self-assembly of two Cu^{II} ions and either two 1,3-phenylenebis(oxamate) (mpba)[11a] or two 1,4-phenylenebis(oxamate) (ppba)[11b] ligands (Chart 1). These anionic $[Cu_2L_2]^{4-}$ complexes (L = mpba and ppba) then serve as building blocks for ladder-type hexanuclear copper(II) and pentanuclear copper(II)−nickel(II) complexes when coordinating to four or three additional M^{II} ions (M = Cu and Ni), respectively, with partially blocked coordination sites.[12] In this respect, APOXA ligands offer a kind of double programming which is responsible for the structure and also for the magnetic properties of the corresponding self-assembling polynuclear complexes.[10] The first level of our ligand programming allows the coordination of the APOXA ligands to the Cu^{II} ions through the bidentate *N*,*O*-oxamato donor groups to give dinuclear copper(II) metallacyclophanes, whereby the Cu^{II} ions are weak to moderate, either ferro- or antiferromagnetically coupled, depending on the meta- or para-substitution pattern of the aromatic phenylene spacers, respectively.[11] The second level of our ligand programming involves the free carbonyl oxygen atoms of the APOXA ligands, which allow these dicopper(II) species to be used as ligands (metalloligands) toward other M^{II} ions (M = Cu and Ni) to give homo- and heterobimetallic penta- and hexanuclear ladders, whereby the Cu^{II} and M^{II} ions are strongly antiferromagnetically coupled through the oxamato bridge.[12]

Chart 1. Heterotopic, Linear Tetranucleating Ligands

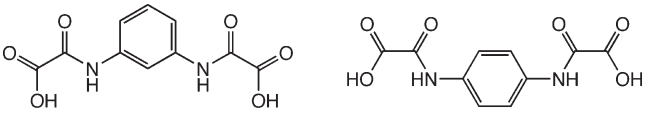

H_4mpba H_4ppba

In this paper, we explore the use of these phenylenedioxamato ligands as tetranucleating bridging ligands for the one-step elaboration of new homo- and heterobimetallic, rack-type tetranuclear cationic complexes of the general formula $[Cu_2M_2LL'_4]^{4+}$ when coordinating to four metal ions of identical or different natures (M = Cu^{II} and/or Ni^{II}) with bi- or tridentate polyamine terminal ligands such as *N*,*N*,*N*′,*N*′-tetramethylethylenediamine (Me_4en) and dipropylenetriamine (dipn), respectively (Chart 2). Here, we report the preparation, crystal structures, and magnetic properties of five tetranuclear copper(II) complexes of formulas $[Cu_4(mpba)(Me_4en)_4(H_2O)_4](ClO_4)_4\cdot 3H_2O$ (**1**), $[Cu_4(mpba)(Me_4en)_4(H_2O)_4](PF_6)_4\cdot 2H_2O$ (**2**), $[Cu_4(ppba)(Me_4en)_4(H_2O)_4](ClO_4)_4\cdot 2H_2O$ (**3**), $[Cu_4(mpba)(dipn)_4](ClO_4)_4\cdot 3H_2O$ (**4**), and $[Cu_4(ppba)(dipn)_4](ClO_4)_4\cdot 2H_2O$ (**5**), together with one tetranuclear copper(II)−nickel(II) complex of formula $[Cu_2Ni_2(ppba)(dipn)_4(H_2O)_2](PF_6)_4$ (**6**). A preliminary communication was already published reporting the unique anion guest interactions in the solid state for **1** and **2**.[13] Herein, we analyze the influence of the nature of the individual metal and ligand constituents (electronic configuration of the metal ion, conformation and substitution pattern of

(2) (a) Fujita, M. *Acc. Chem. Res.* **1999**, *32*, 53. (b) Fujita, M.; Umemoto, K.; Yoshizawa, M.; Fujita, N.; Kusukawa, T.; Biradha, K. *Chem. Commun.* **2001**, 509.

(3) (a) Albrecht, M. *Chem. Soc. Rev.* **1998**, *27*, 281. (b) Albrecht, M.; Janser, I.; Fröhlich, R. *Chem. Commun.* **2005**, 157.

(4) (a) Caulder, D. L.; Raymond, K. N. *J. Chem. Soc., Dalton Trans.* **1999**, 1185. (b) Fiedler, D.; Leung, D. H.; Bergman, R. G.; Raymond, K. N. *Acc. Chem. Res.* **2005**, *38*, 351.

(5) (a) Thompson, L. K. *Coord. Chem. Rev.* **2002**, *233−234*, 193. (b) Dawe, L. N.; Abedin, T. S. M.; Thompson, L. K. *Dalton Trans.* **2008**, 1661.

(6) (a) Lehn, J. M. *Angew. Chem., Int. Ed.* **2004**, *43*, 3644. (b) Ruben, M.; Lehn, J. M.; Muller, P. *Chem. Soc. Rev.* **2006**, *35*, 1056.

(7) (a) Manne, S.; Huttner, G.; Zsolnai, L.; Heinze, K. *Angew. Chem., Int. Ed.* **1996**, *35*, 2808. (b) Fleming, J. S.; Mann, K. L. V.; Carraz, C. A.; Psillakis, E.; Jeffery, J. C.; McCleverty, J. A.; Ward, M. D. *Angew. Chem., Int. Ed.* **1998**, *37*, 1279. (c) McMorran, D. A.; Steel, P. J. *Angew. Chem., Int. Ed.* **1998**, *37*, 3295. (d) Schnebeck, R. D.; Freisinger, E.; Lippert, B. *Angew. Chem., Int. Ed.* **1999**, *38*, 168. (e) Schnebeck, R. D.; Freisinger, E.; Glahé, F.; Lippert, B. *J. Am. Chem. Soc.* **2000**, *122*, 1381. (f) Amouri, H.; Rager, M. N.; Cagnol, F.; Vaissermann, J. *Angew. Chem., Int. Ed.* **2001**, *40*, 3636. (g) Su, C. Y.; Cai, Y. P.; Chen, C. L.; Lissner, F.; Kang, B. S.; Kaim, W. *Angew. Chem., Int. Ed.* **2002**, *41*, 3371. (h) Paul, R. L.; Argent, S. P.; Jeffery, J. C.; Harding, J. P.; Lynam, J. M.; Ward, M. D. *Dalton Trans.* **2004**, 3453. (i) Amouri, H.; Mimassi, L.; Rager, M. N.; Mann, B. E.; Guyard-Duhayon, C.; Raehm, L. *Angew. Chem., Int. Ed.* **2005**, *44*, 4543.

(8) (a) Caulder, D. L.; Powers, R. E.; Parac, T. N.; Raymond, K. N. *Angew. Chem., Int. Ed.* **1998**, *37*, 1840. (b) Parac, T. N.; Caulder, D. L.; Raymond, K. N. *J. Am. Chem. Soc.* **1998**, *120*, 8003. (c) Ziegler, M.; Brumaghin, J. L.; Raymond, K. N. *Angew. Chem., Int. Ed.* **2000**, *39*, 4119.

(9) (a) Fujita, M.; Yu, S. Y.; Kusukawa, T.; Funaki, H.; Ogura, K.; Yamaguchi, Y. *Angew. Chem., Int. Ed.* **1998**, *37*, 2082. (b) Takeda, N.; Umemoto, K.; Yamaguchi, M.; Fujita, M. *Nature (London)* **1999**, *398*, 794. (c) Yu, S. Y.; Kusukawa, T.; Biradha, K.; Fujita, M. *J. Am. Chem. Soc.* **2000**, *122*, 2665. (d) Umemoto, K.; Tsukui, H.; Kusukawa, T.; Biradh, K.; Fujita, M. *Angew. Chem., Int. Ed.* **2002**, *40*, 2620.

(10) Pardo, E.; Ruiz-García, R.; Cano, J.; Ottenwaelder, X.; Lescouezec, R.; Journaux, Y.; Lloret, F.; Julve, M. *Dalton Trans.* **2008**, 2780.

(11) (a) Fernández, I.; Ruiz, R.; Faus, J.; Julve, M.; Lloret, F.; Cano, J.; Ottenwaelder, X.; Journaux, Y.; Muñoz, M. C. *Angew. Chem., Int. Ed.* **2001**, *40*, 3039. (b) Pardo, E.; Faus, J.; Julve, M.; Lloret, F.; Muñoz, M. C.; Cano, J.; Ottenwaelder, X.; Journaux, Y.; Carrasco, R.; Blay, G.; Fernández, I.; Ruiz-García, R. *J. Am. Chem. Soc.* **2003**, *125*, 10770.

(12) (a) Pardo, E.; Bernot, K.; Julve, M.; Lloret, F.; Cano, J.; Ruiz-García, R.; Delgado, F. S.; Ruiz-Pérez, C.; Ottenwaelder, X.; Journaux, Y. *Inorg. Chem.* **2004**, *43*, 2768. (b) Pardo, E.; Ruiz-García, R.; Lloret, F.; Julve, M.; Cano, J.; Pasán, J.; Ruiz-Pérez, C.; Filali, Y.; Chamoreau, L. M.; Journaux, Y. *Inorg. Chem.* **2007**, *46*, 4504.

(13) Pardo, E.; Bernot, K.; Lloret, F.; Julve, M.; Ruiz-García, R.; Pasán, J.; Ruiz-Pérez, C.; Cangussu, D.; Costa, V.; Lescouezec, R.; Journaux, Y. *Eur. J. Inorg. Chem.* **2007**, 4569.

Chart 2. Homo- and Heterobimetallic, Rack-Type Tetranuclear Complexes

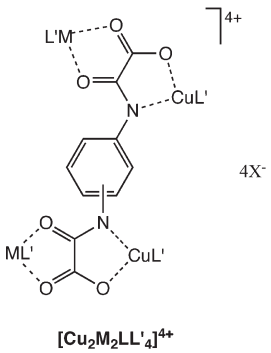

	M	L	L'	X
1	Cu^{II}	mpba	Me_4en	ClO_4^-
2	Cu^{II}	mpba	Me_4en	PF_6^-
3	Cu^{II}	ppba	Me_4en	ClO_4^-
4	Cu^{II}	mpba	dipn	ClO_4^-
5	Cu^{II}	ppba	dipn	ClO_4^-
6	Ni^{II}	ppba	dipn	PF_6^-

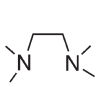

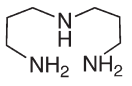

the ligand spacer, and denticity of the terminal ligand) as well as that of the counteranion (size and geometry) on the structure and magnetism of this series of homo- and heterobimetallic tetranuclear racks.

Experimental Section

General. All chemicals were of reagent-grade quality, and they were purchased from commercial sources and used as received. The diethyl ester derivatives of the proligands H_2Et_2L (L = mpba and ppba) were prepared as previously reported.[11]

Caution! *Perchlorate salts containing organic ligands are potentially explosive, and they have to be handled with care and in very small quantities.*

Synthesis of the Complexes. The cationic tetranuclear copper(II) complexes of general formula $[Cu_4LL'_4]^{4+}$ were synthesized in one step by the stoichiometric reaction (1:4) in water of the diethyl ester derivatives of the proligands H_2Et_2L (L = mpba and ppba) previously treated with 4 equiv of NaOH to deprotonate and hydrolyze the amide and ester groups, respectively, with the perchlorate or nitrate salts of the cationic mononuclear copper(II) complexes $[CuL']^{2+}$ (L′ = Me_4en and dipn). These latter species were prepared in situ from a 1:1 mixture of L′ and either $Cu(ClO_4)_2\cdot 6H_2O$ or $Cu(NO_3)_2\cdot 3H_2O$. The cationic tetranuclear copper(II)−nickel(II) complex of general formula $[Cu_2Ni_2LL'_4]^{4+}$ was synthesized in a similar manner by the stoichiometric reaction (1:2:2) of the deprotonated ligand (L = ppba) with the nitrate salt of the cationic mononuclear copper(II) and nickel(II) complexes $[CuL']^{2+}$ and $[NiL']^{2+}$ (L′ = dipn) prepared as mentioned above. They were isolated as perchlorate (**1** and **3**−**5**) or hexafluorophosphate (**2** and **6**) salts by the addition of the stoichiometric amount (1:4) of KPF_6 in the latter case. Satisfactory elemental analyses were obtained for **1**−**6**.

$[Cu_4(mpba)(Me_4en)_4(H_2O)_4](ClO_4)_4\cdot 3H_2O$ (1). An aqueous solution (10 mL) of H_2Et_2mpba (0.08 g, 0.25 mmol) and NaOH (0.04 g, 1.0 mmol) was added dropwise to an aqueous solution (10 mL) of $Cu(ClO_4)_2\cdot 6H_2O$ (0.37 g, 1.0 mmol) and Me_4en (0.15 mL, 1.0 mmol) under continuous stirring. The resulting deep green solution was filtered off and allowed to evaporate at room temperature. X-ray-quality green prisms of **1** were obtained after several days. Yield: 0.28 g (75%). Anal. calcd for $C_{34}H_{82}Cl_4Cu_4N_{10}O_{29}$ (M = 1491): C, 27.36; H, 5.50; N, 9.39. Found: C, 27.06; H, 5.45; N, 9.45. IR (KBr, cm^{-1}): 3419 (O−H), 2986 and 2909 (C−H), 1636 (C═O), 1144, 1113, and 1089 (Cl−O).

$[Cu_4(mpba)(Me_4en)_4(H_2O)_4](PF_6)_4\cdot 2H_2O$ (2). An aqueous solution (10 mL) of H_2Et_2mpba (0.08 g, 0.25 mmol) and NaOH (0.04 g, 1.0 mmol) was added dropwise to an aqueous solution (10 mL) of $Cu(NO_3)_2\cdot 6H_2O$ (0.29 g, 1.0 mmol) and Me_4en (0.15 mL, 1.0 mmol) under continuous stirring. A stoichiometric amount of KPF_6 (0.18 g, 1.0 mmol) was added at the end of the reaction. The resulting deep green solution was filtered off and allowed to evaporate at room temperature. X-ray-quality green prisms of **2** were obtained after several days upon standing. Yield: 0.33 g (80%). Anal. calcd for $C_{34}H_{80}Cu_4F_{24}N_{10}O_{12}P_4$ (M = 1655): C, 24.65; H, 4.83; N, 8.46. Found: C, 24.34; H, 4.72; N, 8.68. IR (KBr, cm^{-1}): 3428 (O−H), 2991 and 2930 (C−H), 1633 (C═O), 841 (P−F).

$[Cu_4(ppba)(Me_4en)_4(H_2O)_4](ClO_4)_4\cdot 2H_2O$ (3). An aqueous solution (10 mL) of H_2Et_2ppba (0.08 g, 0.25 mmol) and NaOH (0.04 g, 1.0 mmol) was added dropwise to an aqueous solution (10 mL) of $Cu(ClO_4)_2\cdot 6H_2O$ (0.37 g, 1.0 mmol) and Me_4en (0.15 mL, 1.0 mmol) under continuous stirring. The resulting deep green solution was filtered off and allowed to evaporate at room temperature. X-ray-quality green prisms of **3** were obtained after several days. Yield: 0.27 g (74%). Anal. calcd for $C_{34}H_{80}Cl_4Cu_4N_{10}O_{28}$ (M = 1473): C, 27.70; H, 5.43; N, 9.50. Found: C, 27.35; H, 5.33; N, 9.61. IR (KBr, cm^{-1}): 3454 (O−H), 2925 (C−H), 1637 (C═O), 1144, 1107, and 1091 (Cl−O).

$[Cu_4(mpba)(dipn)_4](ClO_4)_4\cdot 3H_2O$ (4). An aqueous solution (10 mL) of H_2Et_2mpba (0.08 g, 0.25 mmol) and NaOH (0.04 g, 1.0 mmol) was added dropwise to an aqueous solution (10 mL) of $Cu(ClO_4)_2\cdot 6H_2O$ (0.37 g, 1.0 mmol) and dipn (0.16 mL, 1.0 mmol) under continuous stirring. The resulting deep green solution was filtered off and allowed to evaporate at room temperature. X-ray-quality green prisms of **4** were obtained after several days. Yield: 0.30 g (80%). Anal. calcd for $C_{34}H_{78}Cl_4Cu_4N_{14}O_{25}$ (M = 1480): C, 27.57; H, 5.27; N, 13.24. Found: C, 27.88; H, 5.29; N, 13.47. IR (KBr, cm^{-1}): 3433 (O−H), 3322 and 3260 (N−H), 2986 and 2910 (C−H), 1620 (C═O), 1141, 1114, and 1089 (Cl−O).

$[Cu_4(ppba)(dipn)_4](ClO_4)_4\cdot 2H_2O$ (5). An aqueous solution (10 mL) of H_2Et_2ppba (0.08 g, 0.25 mmol) and NaOH (0.04 g, 1.0 mmol) was added dropwise to an aqueous solution (10 mL) of $Cu(ClO_4)_2\cdot 6H_2O$ (0.37 g, 1.0 mmol) and dipn (0.16 mL, 1.0 mmol) under continuous stirring. The resulting deep green solution was filtered off and allowed to evaporate at room temperature. X-ray-quality green prisms of **5** were obtained after several days. Yield: 0.27 g (75%). Anal. calcd for $C_{34}H_{76}Cl_4Cu_4N_{14}O_{24}$ (M = 1460): C, 27.95; H, 5.21; N, 13.42. Found: C, 27.85; H, 5.13; N, 13.53. IR (KBr, cm^{-1}): 3412 (O−H), 3331 and 3272 (N−H), 2982 and 2912 (C−H), 1634 (C═O), 1141, 1114, and 1089 (Cl−O).

$[Cu_2Ni_2(ppba)(dipn)_4(H_2O)_2](PF_6)_4$ (6). To an aqueous solution (10 mL) of H_2Et_2ppba (0.08 g, 0.25 mmol) and NaOH (0.04 g, 1.0 mmol) were added dropwise, consecutively, two aqueous solutions (10 mL) of $Cu(NO_3)_2\cdot 3H_2O$ (0.12 g, 0.5 mmol) and dipn (0.08 mL, 0.5 mmol), on the one hand, and $Ni(NO_3)_2\cdot 6H_2O$ (0.15 g, 0.5 mmol) and dipn (0.08 mL, 0.5 mmol), on the other hand, under continuous stirring. A stoichiometric amount of KPF_6 (0.18 g, 1.0 mmol) was added at the end of the reaction. The resulting deep green solution was filtered off and allowed to evaporate at room temperature. X-ray-quality green prisms of **6** were obtained after several days. Yield: 0.29 g (72%). Anal. calcd for $C_{34}H_{76}Cu_2F_{24}N_{14}Ni_2O_8P_4$ (M = 1632): C, 25.00; H, 4.66; N, 12.01. Found: C, 25.13; H, 4.53; N, 12.13. IR (KBr, cm^{-1}): 3423 (O−H), 3357 and 3297 (N−H), 2943 and 2889 (C−H), 1586 (C═O), 843 (P−F).

Physical Techniques. Elemental analyses (C, H, N) were performed by the Microanalytical Service of the Universitat de València (Spain). IR spectra were recorded on a Perkin-Elmer 882 spectrophotometer as KBr pellets. Variable-temperature (1.8−300 K) magnetic susceptibility measurements were carried out on powdered samples of **1**−**6** with a Quantum Design SQUID magnetometer. The susceptibility data were corrected for the diamagnetism of both the sample holder and the constituent atoms (Pascal's contants) and for the temperature-indepent paramagnetism of the metal atoms.

Crystal Structure Data Collection and Refinement. X-ray diffraction data of **1**−**6** were collected with graphite-monochromated Mo Kα radiation using a Nonius KappaCCD diffractometer. Crystals of **1** and **3** were somewhat unstable at room temperature. They were mounted at room temperature, and data sets were then collected at 100 K after 1 h to equilibrate the temperature. The crystallographic data show that the crystals remain unaltered upon cooling. At 100 K, we were able to collect suitable single-crystal X-ray data reaching a resolution of 0.9 Å. After trying with different monoclinic space groups for **3** and **4**, the best solutions were obtained for $P2_1/n$ and $I2/m$, respectively.

The structures of **1**−**6** were solved by direct methods and refined with full-matrix least-squares techniques on F^2 using the SHELXS-97 and SHELXL-97 programs.[14a] Data collection and data reduction were done with the COLLECT[14b] and EVALCCD[14c] programs. All calculations for data reduction, structure solution, and refinement were done by standard procedures (WINGX).[14d] The final geometrical calculations and the graphical manipulations were carried out with the PARST97[14e] and CRYSTAL MAKER[14f] programs, respectively. All non-hydrogen atoms were refined anisotropically. The hydrogen atoms of the organic ligands were set on calculated positions and refined with a riding model, while those of the water molecules were neither found nor calculated. The structures of **3** and **4** exhibit disordered positions for the phenylene ring of the mpba and ppba ligands. In **3**, two disordered positions appear in the asymmetric unit, and they were refined with variable soluble organic fractions, leading to occupations of 0.64 and 0.36 for each of the configurations. In **4**, the disorder appears as a consequence of symmetry operations, and the occupation was then fixed to 0.5. The two crystallographically independent perchlorate anions in **5** and the carbon atom C(6) of a dipn ligand in **6** are also disordered. A summary of the crystallographic data for **1**−**6** is listed in Table 1. Selected bond distances for **1**−**6** are listed in Tables 2−7.

Results and Discussion

Description of the Structures. $[Cu_4(mpba)(Me_4en)_4(H_2O)_4](ClO_4)_4\cdot 3H_2O$ (1). The structure of **1** consists of tetranuclear cationic copper(II) complexes, $[Cu_4(mpba)(Me_4en)_4(H_2O)_4]^{4+}$, perchlorate anions, and crystallization water molecules (Figure 1).

The tetracopper(II) cations exhibit an overall ^{4}R rack-type architecture formed by four $[Cu(Me_4en)(H_2O)]^{2+}$ subunits connected by one tetrakis(bidentate) mpba ligand. Because of its rotational freedom, this bridging ligand adopts a nonplanar helical conformation with the two oxamato bridging groups tilted up and down with respect to the plane of the *m*-phenylene spacer (*anti* configuration). The values of the torsion angle around the N(amide)−C(phenylene) bonds (ϕ) are 91.0(3) and 108.8(4)°, values which are greater than that of H_2Et_2-mpba [ϕ = 32.6(5)°].[15a] This gives rise to chiral bis-binuclear entities of pseudo-2-fold symmetry, either *M* or *P* helical conformers, which are made up of two oxamato-bridged Cu_2^{II} units connected through a *meta*-phenylenediamidato bridge between one of the two copper atoms of each binuclear unit (Figure 1a). The intradimer distance (d) between the copper atoms through the oxamato bridge averages to 5.190(2) Å, whereas the interdimer distance (d') through the *meta*-phenylenediamidato bridge is 7.762(2) Å.

The four crystallographically independent copper atoms of **1** exhibit square-pyramidal geometries, CuN_3O_2 for Cu(1) and Cu(3) and CuN_2O_3 for Cu(2) and Cu(4), with axially coordinated water molecules [Cu−Ow = 2.284(6)−2.521(9) Å] which are arranged in a *trans* position within each binuclear unit (Figure 1b). The two oxamato groups of the mpba ligand coordinate through the amidate-nitrogen and carboxylate-oxygen atoms to the Cu(1) and Cu(3) atoms [Cu−N = 1.997(6)−2.012(7) Å; Cu−O = 1.978(7)−2.004(7) Å] and through the carbonyl-oxygen atoms to the Cu(2) and Cu(4) atoms [Cu−O = 1.947(6)−1.965(6) Å], whereas the remaining positions of the equatorial plane are occupied by two amine-nitrogen atoms from the Me_4en ligands [Cu−N = 1.994(7)−2.059(7) Å]. The copper basal planes and the oxamato plane of each binuclear unit are quite coplanar, the values of the dihedral angle (ψ) between the copper basal planes and the oxamato plane being in the range 3.8(2)−17.7(2)°. Because of the meta topology of the ligand spacer, the mean planes of the two oxamato bridging groups form a dihedral "bite" angle of 54.5(2)°, conferring thus a global bowl-like shape to the tetracopper(II) cations (Figure 1b).

Interestingly, two symmetry-related, bowl-shaped tetracopper(II) cations of opposite chirality encapsulate two perchlorate anions, yielding a centrosymmetric heterochiral (*P*,*M* mesomer) dimeric capsule (Figure 1c). The encapsulated ClO_4^- anions establish weak dative interactions with the coordinatively unsaturated copper atoms [Cu−O = 2.894(2) Å], together with hydrogen bonds with the axially coordinated water molecules pointing toward the inner side of the capsule [Ow−O = 2.977(9) Å]. The two encapsulated ClO_4^- anions occupy equivalent positions within the confined space of the capsule [Cl(3)−Cl(3^I) = 5.247(4) Å]. The intermolecular distances between the equivalent copper atoms from each tetranuclear cation are in the narrow range 9.988(2)−14.626(2) Å, values which can be taken as the approximate dimensions of this nanometer-sized metallosupramolecular capsule.

In the crystal lattice, some of the nonencapsulated ClO_4^- anions also establish weak coordinative bonds with the copper atoms [Cu−O = 2.874(8) Å] and hydrogen bonds with the axially coordinated water molecules pointing toward the outer side of the capsule [Ow−O = 2.563(8)−2.918(8) Å]. This situation leads to a rather close packing of the spherical-shaped capsules (Figure S1, Supporting Information).

$[Cu_4(mpba)(Me_4en)_4(H_2O)_4](PF_6)_4\cdot 2H_2O$ (2). The structure of **2** consists of tetranuclear copper(II) cations, $\{[Cu_4(mpba)(Me_4en)_4(H_2O)_4\}^{4+}$, hexafluorophosphate anions, and crystallization water molecules (Figure 2).

The tetracopper(II) cations exhibit an overall ^{4}R rack-type architecture which is configurationally identical to that observed for **1**. The four $[Cu(Me_4en)(H_2O)]^{2+}$ subunits are connected by the tetrakis(bidentate) mpba ligand with an

(14) (a) Sheldrick, G. M. *SHELX97*, release 97-2; Institut fur Anorganische Chemie der Universität Göttingen: Göttingen, Germany, **1998**. (b) Hooft, R. W. W. *COLLECT*; Nonius BV: Delft, The Netherlands, **1999**. (c) Duisenberg, A. J. M.; Kroon-Batenburg, L. M. J.; Schreurs, A. M. M. *J. Appl. Crystallogr.* **2003**, *36*, 220(EVALCCD). (d) Farrugia, L. J. *J. Appl. Crystallogr.* **1999**, *32*, 837(*WINGX*). (e) Nardelli, M. *J. Appl. Crystallogr.* **1995**, *28*, 659. (f) Palmer, D. *CRYSTAL MAKER*; Cambridge University Technical Services: Cambridge, U.K., **1996**.

(15) (a) Blay, G.; Fernández, I.; Pedro, J. R.; Ruiz-García, R.; Muñoz, M. C.; Cano, J.; Carrrasco, R. *Eur. J. Org. Chem.* **2003**, *9*, 1627. (b) Yang, W.; Liu, X. *Acta Crystallogr.* **2008**, *E64*, o1852.

Table 1. Summary of Crystallographic Data for **1**−**6**

	1	**2**	**3**	**4**	**5**	**6**
formula	$C_{34}H_{82}Cl_4Cu_4N_{10}O_{29}$	$C_{34}H_{80}Cu_4F_{24}N_{10}O_{12}P_4$	$C_{17}H_{40}Cl_2Cu_2N_5O_{14}$	$C_{34}H_{78}Cl_4Cu_4N_{14}O_{25}$	$C_{34}H_{76}Cl_4Cu_4N_{14}O_{24}$	$C_{34}H_{76}F_{24}Cu_2Ni_2N_{14}O_8P_4$
M (g mol^{-1})	1491.06	1655.12	736.52	1480.01	1470.89	1633.31
cryst syst	triclinic	monoclinic	monoclinic	monoclinic	monoclinic	monoclinic
space group	$P\bar{1}$	$C2/c$	$P2_1/n$	$I2/m$	$P2_1/a$	$P2_1/a$
a (Å)	14.3494(9)	16.045(2)	11.541(2)	13.2249(9)	14.7259(10)	14.981(3)
b (Å)	14.8957(15)	26.659(2)	18.301(8)	32.895(3)	12.4941(4)	13.134(3)
c (Å)	15.1787(19)	30.758(3)	15.371(6)	14.4976(11)	15.7297(10)	15.911(3)
α (deg)	70.862(8)	90.0	90.0	90.0	90.0	90.0
β (deg)	86.966(6)	96.187(10)	110.521(7)	96.082(6)	100.043(3)	100.964(8)
γ (deg)	88.797(6)	90.0	90.0	90.0	90.0	90.0
V (Å^3)	3060.7(5)	13080(3)	3040.5(19)	6271.5(9)	2849.7(3)	3073.6(11)
Z	2	8	4	4	2	2
ρ_{calcd} (g cm^{-3})	1.618	1.681	1.609	1.559	1.679	1.743
$F(000)$	1544	6736	1524	3028	1468	1624
μ (mm^{-1})	1.634	1.506	1.643	1.592	1.748	1.519
T (K)	100(2)	293(2)	100(2)	293(2)	293(2)	293(2)
R^a [$I > 2\sigma(I)$]	0.0743	0.0854	0.1213	0.0830	0.0728	0.0749
wR^b [$I > 2\sigma(I)$]	0.1920	0.1379	0.2865	0.2363	0.1847	0.1854
S^c	1.058	1.013	1.317	1.032	1.106	1.029

[a] $R = \sum(|F_o| - |F_c|)/\Sigma|F_o|$. [b] $wR = [\sum w(|F_o| - |F_c|)^2/\sum w|F_o|^2]^{1/2}$. [c] $S = [\sum w(|F_o| - |F_c|)^2/(N_o - N_p)]^{1/2}$.

Table 2. Selected Bond Distances (Å) for **1**[a]

Cu(1)−O(3)	2.004(6)	Cu(1)−N(3)	2.047(8)
Cu(1)−N(1)	1.997(6)	Cu(1)−N(4)	2.039(7)
Cu(1)−O(1w)	2.286(7)	Cu(2)−O(2)	1.960(6)
Cu(2)−O(1)	1.965(6)	Cu(2)−N(5)	2.011(8)
Cu(2)−O(2w)	2.397(12)	Cu(2)−N(6)	2.006(8)
Cu(3)−O(4)	1.978(7)	Cu(3)−N(7)	2.040(7)
Cu(3)−N(2)	2.012(7)	Cu(3)−N(8)	2.059(7)
Cu(3)−O(3w)	2.284(6)	Cu(4)−O(5)	1.987(8)
Cu(4)−O(6)	1.947(6)	Cu(4)−N(9)	1.994(7)
Cu(4)−N(10)	2.014(9)	Cu(4)−O(4w)	2.521(9)

[a] The estimated standard deviations are given in parentheses.

Table 3. Selected Bond Distances (Å) for **2**[a]

Cu(1)−O(3)	1.984(5)	Cu(1)−N(3)	2.054(7)
Cu(1)−N(1)	2.004(7)	Cu(1)−N(4)	2.052(7)
Cu(1)−O(1w)	2.364(7)	Cu(2)−O(2)	1.996(6)
Cu(2)−O(1)	1.962(5)	Cu(2)−N(5)	2.006(7)
Cu(2)−O(2w)	2.386(7)	Cu(2)−N(6)	2.036(8)
Cu(3)−O(4)	2.002(6)	Cu(3)−N(7)	2.049(7)
Cu(3)−N(2)	2.001(6)	Cu(3)−N(8)	2.061(8)
Cu(3)−O(3w)	2.415(8)	Cu(4)−O(5)	1.978(6)
Cu(4)−O(6)	1.951(5)	Cu(4)−N(9)	2.025(7)
Cu(4)−N(10)	2.000(7)	Cu(4)−O(4w)	2.460(6)

[a] The estimated standard deviations are given in parentheses.

Table 4. Selected Bond Distances (Å) for **3**[a]

Cu(1)−O(3)	1.987(7)	Cu(1)−N(1)	1.948(9)
Cu(1)−N(2)	2.022(11)	Cu(1)−N(3)	2.004(11)
Cu(1)−O(1w)	2.383(9)	Cu(2)−O(2)	1.981(7)
Cu(2)−O(1)	1.949(10)	Cu(2)−N(4)	2.023(10)
Cu(2)−N(5)	2.031(10)	Cu(2)−O(2w)	2.374(10)

[a] The estimated standard deviations are given in parentheses.

Table 5. Selected Bond Distances (Å) for **4**[a]

Cu(1)−O(3)	2.194(5)	Cu(1)−N(1)/O(1B)	2.026(5)
Cu(1)−N(2)	2.021(6)	Cu(1)−N(3)	2.034(6)
Cu(1)−N(4)	1.999(7)	Cu(2)−O(2)	2.208(5)
Cu(2)−O(1)/N(1B)	2.019(5)	Cu(2)−N(5)	2.004(7)
Cu(2)−N(6)	2.010(6)	Cu(2)−N(7)	2.011(6)

[a] The estimated standard deviations are given in parentheses.

Table 6. Selected Bond Distances (Å) for **5**[a]

Cu(1)−O(3)	2.183(3)	Cu(1)−N(1)	2.014(4)
Cu(1)−N(2)	2.050(4)	Cu(1)−N(3)	2.038(5)
Cu(1)−N(4)	2.046(5)	Cu(2)−O(2)	2.059(3)
Cu(2)−O(1)	2.155(3)	Cu(2)−N(5)	2.011(4)
Cu(2)−N(6)	2.029(5)	Cu(2)−N(7)	2.014(4)

[a] The estimated standard deviations are given in parentheses.

Table 7. Selected Bond Distances (Å) for **6**[a]

Cu(1)−O(3)	2.155(5)	Cu(1)−N(1)	2.025(4)
Cu(1)−N(2)	2.032(6)	Cu(1)−N(3)	2.024(6)
Cu(1)−N(4)	2.035(7)	Ni(1)−O(2)	2.116(4)
Ni(1)−O(1)	2.087(4)	Ni(1)−N(5)	2.069(5)
Ni(1)−N(6)	2.087(5)	Ni(1)−N(7)	2.074(6)
Ni(1)−O(1w)	2.122(5)		

[a] The estimated standard deviations are given in parentheses.

anti nonplanar helical conformation leading to chiral bis-binuclear entities of pseudo-2-fold symmetry (*M* or *P* helical conformers), which are made up of two oxamato-bridged Cu_2^{II} units connected through a *meta*-phenylenediamidate bridge between one of the two copper atoms of each binuclear unit (Figure 2a). The values of the torsion angle around the N(amide)−C(phenylene) bonds (ϕ) are 90.7(5) and 112.7(6)°, values which are similar to those reported for **1**. The intradimer distance (d) between the copper atoms through the oxamato bridge averages to 5.224(2) Å, whereas the interdimer distance (d') through the *meta*-phenylenediamidato bridge is 7.571(2) Å.

The four crystallographically independent copper atoms of **2** exhibit square-pyramidal geometries, CuN_3O_2 for Cu(1) and Cu(3) and CuN_2O_3 for Cu(2) and Cu(4), with axially coordinated water molecules [Cu−Ow = 2.364(7)−2.460(6) Å] which are arranged in a *trans* position within each binuclear unit (Figure 2b). The two oxamato groups of the mpba ligand are coordinated to Cu(1) and Cu(3) atoms through the amidate-nitrogen and carboxylate-oxygen atoms [Cu−N = 2.001(6)−2.004(7) Å; Cu−O = 1.984(5)−2.002(6) Å] and through the carbonyl-oxygen atoms to Cu(2) and Cu(4)

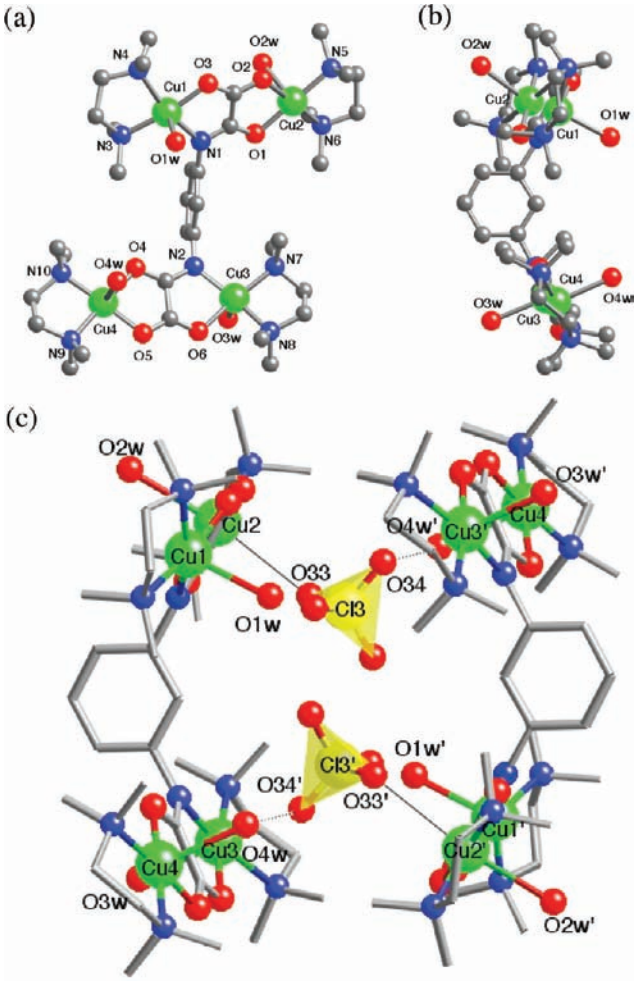

Figure 1. (a) Front and (b) side views of the cationic tetranuclear unit of **1** with the atom numbering scheme for the metal coordination environments (hydrogen atoms are omitted for clarity). (c) Perspective view of the dimeric capsule of tetranuclear entities with coordinated and hydrogen-bonded encapsulated perchlorate anions (coordinative and hydrogen bonds are drawn as solid and dotted lines, respectively) (I = $-x, -y, -z$; II = $-x, y, 1/2 - z$).

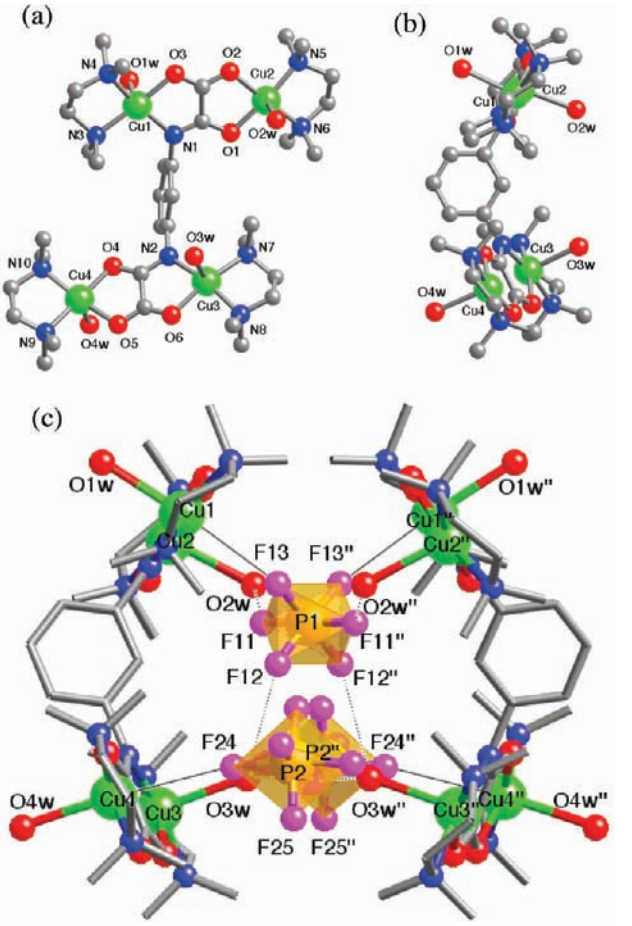

Figure 2. (a) Front and (b) side views of the cationic tetranuclear unit of **2** with the atom numbering scheme for the metal coordination environments (hydrogen atoms are omitted for clarity). (c) Perspective view of the dimeric capsule of tetranuclear entities with coordinated and hydrogen-bonded encapsulated hexafluorophosphate anions (coordinative and hydrogen bonds are drawn as solid and dotted lines, respectively) (I = $-x, -y, -z$; II = $-x, y, 1/2 - z$).

[Cu−O = 1.951(5)−1.996(6) Å]; the remaining positions of the equatorial plane at each copper atom are occupied by two amine-nitrogen atoms from the Me_4en ligands [Cu−N = 2.000(7)−2.061(8) Å]. The copper basal planes and the oxamato plane of each binuclear unit are quite coplanar [ψ = 6.7(2)−11.2(2)°]. The two mean planes of the two oxamato bridging groups form a dihedral "bite" angle of 53.9(1)°, conferring a global bowl-like shape to the tetracopper(II) cations as found for **1** (Figure 2b).

Unlike **1**, two symmetry-related, bowl-shaped tetracopper(II) cations of identical chirality encapsulate three hexafluorophosphate anions, yielding a centrosymmetric racemic mixture of 2-fold homochiral (*P*,*P* and *M*,*M* enantiomers) dimeric capsules (Figure 2c). The diastereoisomer differentiation that occurs in these 2:2 (**1**) and 2:3 (**2**) host−guest complexes, $\{meso\text{-}(ClO_4)_2\subset[Cu_4(mpba)(Me_4en)_4(H_2O)_4]_2\}^{2+}$ and $\{rac\text{-}(PF_6)_3\subset[Cu_4(mpba)(Me_4en)_4(H_2O)_4]_2\}^{+}$, respectively, is most likely related to the different size and geometry of the perchlorate and hexafluorophosphate anions. The encapsulated PF_6^- anions establish the same sort of interactions that occur in **1**, which means very weak interactions with the coordinatively unsaturated copper atoms [Cu−F = 3.044(8)−3.221(8) Å], together with hydrogen bonds with the axially coordinated water molecules pointing toward the inner side of the capsule [Ow−F = 2.858(8)−2.933(8) Å] (Figure 2c). These coordinative and hydrogen-bonding interactions between the cationic hosts and the anionic guests contribute to stabilize the resulting noncovalent capsules, together with the host−guest Coulombic attractions. The three encapsulated PF_6^- anions in **2** exhibit a triangular arrangement with the edges of the isosceles triangle defined by P(1)−P(2) and P(2)−P(2^{II}) distances of 5.632(6) and 8.898(7) Å, respectively. The intermolecular distances between the equivalent copper atoms from each tetranuclear cation are in the range of 7.031(2)−14.135(2) Å, values which are broader than those of **1**, resulting thus in a slightly open configuration of the metallosupramolecular capsule in **2**.

In the crystal lattice, some of the nonencapsulated PF_6^- anions weakly interact with the copper atoms [Cu−F = 3.411(8) Å] and with the axially coordinated water molecules pointing toward the outer side of the capsule [Ow−F = 2.951(8)−2.959(8) Å]. This situation leads to a rather close packing of the spherically shaped capsules in **2**, as previously observed in **1** (Figure S2, Supporting Information). Most likely, these intermolecular interactions

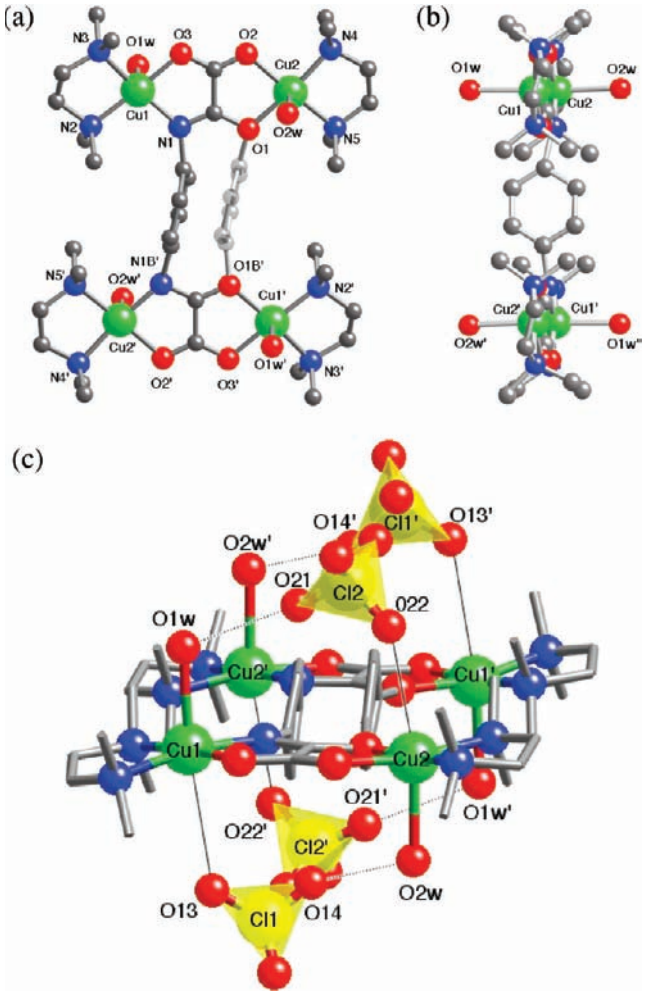

Figure 3. (a) Front and (b) side views of the cationic tetranuclear unit of **3** with the atom numbering scheme for the metal coordination environments (hydrogen atoms are omitted for clarity). (c) Perspective view of the wagonwheel tetranuclear entity with coordinated and hydrogen-bonded perchlorate anions (coordinative and hydrogen bonds are drawn as solid and dotted lines, respectively) showing the two centrosymmetrically related phenylene rings resulting from structural disorder (I = $2 - x, -y, 1 - z$).

can play a non-negligible role in the different metallosupramolecular structural motifs of **1** and **2**.

$[Cu_4(ppba)(Me_4en)_4(H_2O)_4](ClO_4)_4 \cdot 2H_2O$ (3). The structure of **3** consists of disordered tetranuclear copper(II) cations, $[Cu_4(ppba)(Me_4en)_4(H_2O)_4]^{4+}$, perchlorate anions, and crystallization water molecules (Figure 3). Because of the disorder in **3** (see Experimental Section), two centrosymmetrically related phenylene rings with 0.64 and 0.36 occupancy factors of the carbon atoms virtually picture a paracyclophane-type structure for the ppba ligand within the tetracopper(II) cation (Figure 3c).

The tetracopper(II) cations, with a crystallographically imposed C_i symmetry, are formed by four $[Cu(Me_4en)(H_2O)_4]^{2+}$ subunits connected by the tetrakis(bidentate) ppba ligand, thus resulting in achiral bis-binuclear entities with an overall ^{4}R rack-type architecture (Figure 3a). As for **1** and **2**, the ppba bridging ligand adopts a nonplanar conformation in order to prevent the steric hindrance between the *para*-phenylene spacer and the "in-plane" Me_4en ligands belonging to each of the two oxamato-bridged Cu_2^{II} units (Figure 3b). However, the two oxamato groups of the ppba ligand in **3** are tilted toward the same side with respect to the plane of the *p*-phenylene spacer (*syn* configuration), unlike in **1** and **2** where they are tilted toward opposed sides with respect to the plane of the *m*-phenylene spacer (anti configuration). The values of 98(2)° and 99(2)° for the torsion angles around the N(amide)−C(phenylene) bond are within the range of those reported for **1** and **2** [ϕ = 90.7(5)−112.7(6)°]. The intradimer distance (d) between the copper atoms through the oxamato bridge in **3** is 5.185(2) Å, whereas the interdimer one (d') through the *para*-phenylenediamidato bridge is 8.319(4) Å.

The two crystallographically independent copper atoms of **3** exhibit a square-pyramidal geometry with two possible CuN_3O_2 and CuN_2O_3 chromophores for both Cu(1) and Cu(2) because of the structural disorder. The two oxamato groups of the ppba ligand are coordinated to each copper atom through the amidate-nitrogen and the carboxylate- and carbonyl-oxygen atoms [Cu−N/O = 1.948(11)−1.947(9) Å and Cu−O = 1.987(7)−1.980(9) Å], the remaining equatorial positions being occupied by two amine-nitrogen atoms from the Me_4en ligands [Cu−N = 2.004(14)−2.031(15) Å]. The axially coordinated water molecules [Cu−Ow = 2.374(10)−2.383(9) Å] are arranged in a *trans* position within each binuclear unit (Figure 3a). The copper basal planes and the oxamato plane of each binuclear unit are quite coplanar [ψ = 5.4(2) and 9.3(2)° for Cu(1) and Cu(2), respectively]. Interestingly, the four ClO_4^- anions establish very weak dative interactions with the coordinatively unsaturated copper atoms [Cu−O = 3.18(3)−3.400(19) Å], together with hydrogen bonds with the axially coordinated water molecules of the neighboring copper atom within each binuclear unit [O(1w)−O(5) = 2.70(2) Å and O(2w)−O(11) = 2.80(2) Å] (Figure 3c). This 4-fold handle-shaped motif leads to a global wagonwheel tetranuclear entity, whereby the ppba bridging ligand acts as an "axis" between the two metallacyclic $[Cu(Me_4en)(H_2O)(ClO_4)]_2^{2+}$ binuclear units, which then serve as "wheels" (Figure 3c).

A rather close packing of these wagonwheel-shaped tetranuclear entities occurs in the crystal lattice of **3** due to the presence of a variety of intermolecular hydrogen-bonding interactions involving the perchlorate anions and both the coordinated and crystallization water molecules (Figure S3, Supporting Information). So, the weakly coordinated ClO_4^- anions are hydrogen-bonded to the axially coordinated water molecules of the copper atoms from neighboring tetranuclear entities [Ow−O = 2.99(3) Å]. They are further connected through hydrogen bonds involving the crystallization and coordinated water molecules and the carbonyl- or carboxylate-oxygen atoms from the oxamato groups [Ow−Ow = 2.836(17) Å and Ow−O = 3.04(3)−3.074(15) Å].

$[Cu_4(mpba)(dipn)_4](ClO_4)_4 \cdot 3H_2O$ (4). The structure of **4** consists of disordered tetranuclear copper(II) cations, $[Cu_4(mpba)(dipn)_4]^{4+}$, perchlorate anions, and crystallization water molecules (Figure 4). As a result of severe disorder problems in **4** (see Experimental Section), two centrosymmetrically related tetranuclear copper(II) cations virtually picture a dimeric aggregate with a biphenylenophane-type linking motif which is made up

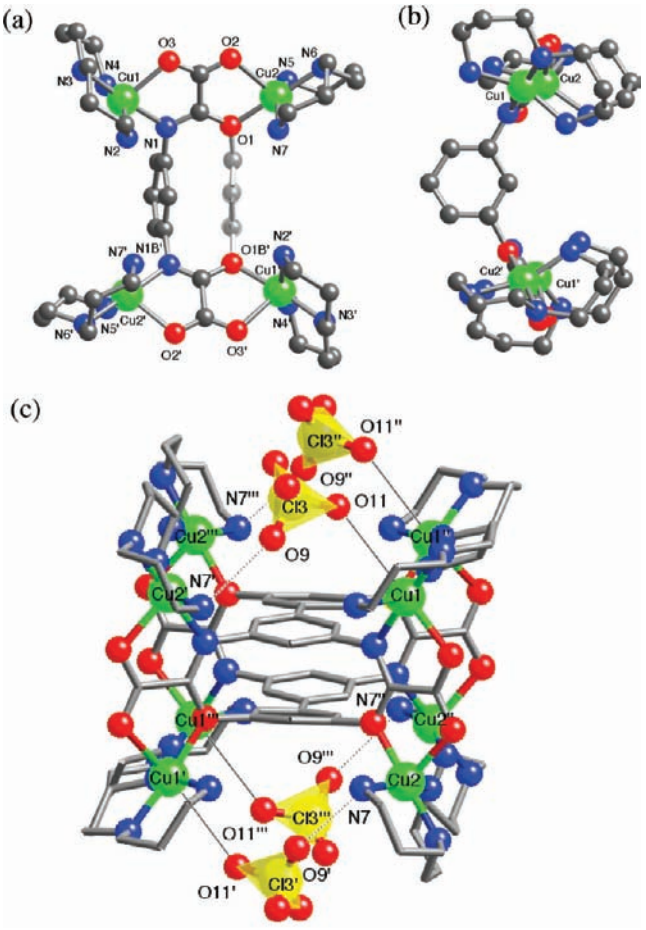

Figure 4. (a) Front and (b) side views of the cationic tetranuclear unit of **4** with the atom numbering scheme for the metal coordination environments (hydrogen atoms are omitted for clarity). (c) Perspective view of the wagonwheel dimer of tetranuclear entities with coordinated and hydrogen-bonded perchlorate anions (coordinative and hydrogen bonds are drawn as solid and dotted lines, respectively) showing the two centrosymmetrically related biphenylene rings resulting from structural disorder (I = 2 − *x*, *y*, −*z*; II = *x*, 2 − *y*, *z*; III = 2 − *x*, 2 − *y*, −*z*).

of two pairs of centrosymmetrically related phenylene rings from each mpba ligand with a half-occupancy factor of the carbon atoms (Figure 4c).

The tetracopper(II) cations, with a crystallographically imposed C_2 symmetry, are formed by four $[Cu(dipn)]^{2+}$ subunits connected by the tetrakis(bidentate) mpba ligand in a *syn* nonplanar conformation, leading thus to achiral (nonhelical) bis-binuclear entities with an overall ^{4}R rack-type architecture (Figure 4a). This situation contrasts with that found in **1** and **2** where the mpba ligand exhibits an anti nonplanar helical conformation leading to chiral bis-binuclear entities. The value of 82.1(11)° for the torsion angle around the N(amide)−C(phenylene) bond is close to those reported for **1** and **2** [ϕ = 90.7(5)−112.7(6)°]. The intradimer distance (d) between the copper atoms through the oxamato bridge in **4** is 5.4906(12) Å, whereas the interdimer one (d') through the *meta*-phenylenediamidato bridge is 6.9589(12) Å.

The two crystallographically independent copper atoms of **4** exhibit a slightly distorted square-pyramidal geometry with two possible CuN_4O and CuN_3O_2 chromophores for both Cu(1) and Cu(2) because of disorder reasons. The values of the trigonalization parameter (τ) are 0.40 [Cu(1)] and 0.35 [Cu(2)] (τ = 0 and 1 for ideal square-pyramidal and trigonal-bipyramidal geometries, respectively).[16] The basal plane at each copper atom is formed by three amine-nitrogen atoms of the dipn ligand in a *mer* conformation [Cu(1)−N = 2.000(7)−2.034(6) Å and Cu(2)−N = 2.004(7)−2.011(6) Å] and an amidate-nitrogen or a carbonyl amidate-oxygen atom from the oxamato group of the mpba bridging ligand [Cu(1)−N(1)/O(1B) = 2.026(4) Å and Cu(2)−N(1B)/O(1) = 2.019(4) Å], while the axial position is occupied by the carbonyl- and carboxylate-oxygen atoms [Cu(1)−O(3) = 2.194(5) Å and Cu(2)−O(2) = 2.207(4) Å] (Figure 4a). The basal planes of the copper atoms in **4** are then disposed on the same side of the oxamato group, and they are almost perpendicular to the oxamato plane [ψ = 89.02(16) and 84.76(18)° for Cu(1) and Cu(2), respectively]. This side-by-side "out-of-plane" disposition contrasts with that found in **1** and **2** where the copper basal planes and the oxamato plane of each binuclear unit are coplanar [ψ = 3.8(2)−17.7(2)°].

Within each of the two centrosymmetrically related tetranuclear copper(II) cations which conform the dimeric aggregate resulting from the structural disorder of the mpba bridging ligand, the ClO_4^- anions establish weak dative interactions with the coordinatively unsaturated copper atoms from one binuclear unit [Cu(1)−O(11) = 3.300(9) Å] and intramolecular N−H···O hydrogen bonds with the coordinated amine groups of the dipn ligand from another binuclear unit [N−O = 3.080(9)−3.231(17) Å] (Figure 4c). In addition, the tetranuclear units are linked through intermolecular N−H···O hydrogen bonds involving a carboxylate-oxygen atom and an amino-nitrogen atom from the dipn ligand [N(6)−O(2) = 2.938(7) Å] to form chains along the *a* axis. The close packing of these bis(tetranuclear) entities in the crystal lattice leads to small pores along the *c* axis which are occupied by noncoordinated ClO_4^- anions and hydrogen-bonded crystallization water molecules [Ow−Ow = 2.72(3)−2.94(3) Å and Ow−O = 3.14(3)−3.16(3) Å] (Figure S4, Supporting Information).

$[Cu_4(ppba)(dipn)_4](ClO_4)_4\cdot 2H_2O$ (5). The structure of **5** consists of tetranuclear copper(II) cations, $[Cu_4(ppba)(dipn)_4]^{4+}$, perchlorate anions, and crystallization water molecules (Figure 5). The tetracopper(II) cations are formed by four $[Cu(dipn)]^{2+}$ subunits connected by the tetrakis(bidentate) ppba ligand to give a centrosymmetric bis-binuclear entity with an overall ^{4}R rack-type architecture (Figure 5a). In contrast to **3**, the ppba ligand adopts a more favorable *anti* planar conformation because of the absence of steric hindrance between the *para*-phenylene spacer and the "out-of-plane" dipn ligand belonging to each of the two oxamato-bridged Cu_2^{II} units (Figure 5b). The torsion angle around the N(amide)−C(phenylene) bond (ϕ) is 12.7(7)°, a value which is smaller than that of H_2Et_2ppba [ϕ = 34.6(5)°].[15b] The intradimer distance (d) between the copper atoms through the oxamato bridge in **5** is 5.5040(8) Å, whereas the interdimer one (d') through the *para*-phenylenediamidato bridge is 8.4540(9) Å.

The two crystallographically independent copper atoms of **5** exhibit a slightly distorted square-pyramidal

(16) Costa, R.; García, A.; Ribas, J.; Mallah, T.; Journaux, Y.; Sletten, J.; Solans, X. *Inorg. Chem.* **1993**, *32*, 3733.

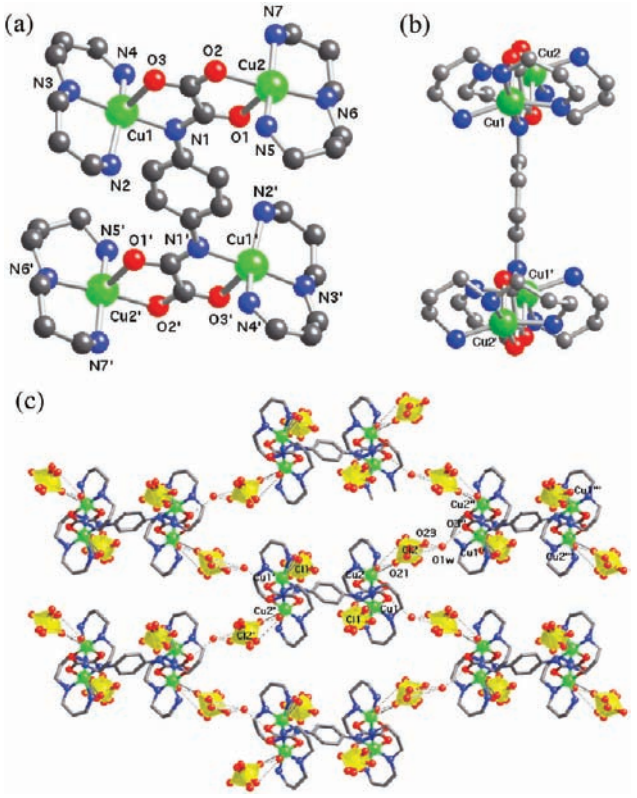

Figure 5. (a) Front and (b) side views of the cationic tetranuclear unit of **5** with the atom numbering scheme for the metal coordination environments (hydrogen atoms are omitted for clarity). (c) Perspective view of a fragment of the layer of tetranuclear entities with coordinated and hydrogen-bonded percchlorate anions (coordinative and hydrogen bonds are drawn as solid and dotted lines, respectively) (I = $-x$, $1-y$, $1-z$; II = $1/2-x$, $1/2+y$, $-z$; III = $1/2+x$, $3/2-y$, $-1+z$).

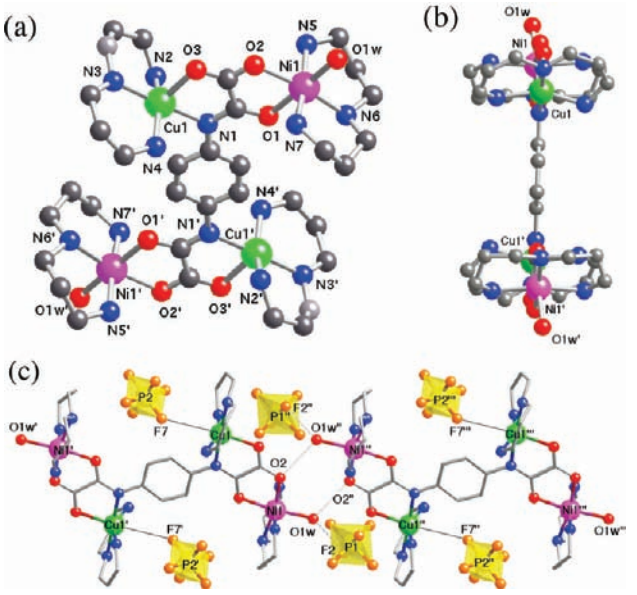

Figure 6. (a) Front and (b) side views of the cationic tetranuclear unit of **6** with the atom numbering scheme for the metal coordination environments (hydrogen atoms are omitted for clarity). (c) Perspective view of a fragment of the chain of tetranuclear entities with coordinated and hydrogen-bonded hexafluorophosphate anions (coordinative and hydrogen bonds are drawn as solid and dotted lines, respectively) (I = $-x$, $1-y$, $-z$; II = $-x$, $1-y$, $1-z$; III = x, y, $1+z$).

geometry, CuN_4O for Cu(1) and CuN_3O_2 for Cu(2). The values of τ are 0.40 [Cu(1)] and 0.29 [Cu(2)], values which are similar to those found in **4** (τ = 0.40 and 0.35). The basal plane at Cu(1) is formed by three amine-nitrogen atoms of the dipn ligand in a *mer* conformation [Cu(1)−N = 2.039(5)−2.050(5) Å] and an amidate-nitrogen atom from the oxamato group of the ppba bridging ligand [Cu(1)−N(1) = 2.014(4) Å], while the axial position is occupied by a carboxylate-oxygen atom [Cu(1)−O(3) = 2.183(3) Å]. The basal plane at Cu(2) is formed by three amine-nitrogen atoms of the dipn ligand in a *mer* conformation [Cu(2)−N = 2.011(5)−2.029(4) Å] and a carbonyl carboxylate-oxygen atom from the oxamato group [Cu(2)−O(2) = 2.058(3) Å], while the other carbonyl amidate-oxygen atom occupies the axial position [Cu(2)−O(1) = 2.155(3) Å] (Figure 5a). The basal planes at the copper atoms in **5** are then disposed on opposite sides of the oxamato group, as compared to the side-by-side disposition found in **4**. However, they are almost perpendicular to the plane of the oxamato group [ψ = 82.22(12) and 86.08(12)° for Cu(1) and Cu(2), respectively] as in **4** [ψ = 89.02(16) and 84.76(18)°] (Figure 5b). This situation contrasts with that found in **1**−**3** where the copper basal planes and the oxamato plane of each binuclear unit are coplanar [ψ = 3.8(2)−17.7(2)°].

The four perchlorate anions are weakly coordinated to the copper atoms [Cu−O = 3.021(15)−3.36(3) Å] as in **4** (Figure 5c). In addition, the tetranuclear cations are connected through hydrogen bonds between the weakly coordinated ClO_4^- anions and the carboxylate-oxygen atoms from oxamato groups through the crystallization water molecules [O(1w)−O(3) = 2.872(11) Å and O(1w)−O(23A) = 3.17(3) Å] leading to rhombic layers (Figure 5c). The value of the shortest intermolecular copper−copper distance between neighboring Cu_4^{II} entities is 10.4117(9) Å. In the crystal lattice, the packing of these layers of Cu_4^{II} entities leads to small pores along the *a* axis which are occupied by both the weakly coordinated and hydrogen-bonded ClO_4^- anions (Figure S5, Supporting Information).

$[Cu_2Ni_2(ppba)(dipn)_4(H_2O)_2](PF_6)_4$ (6). The structure of **6** consists of tetranuclear copper(II)−nickel(II) cations, $[Cu_2Ni_2(ppba)(dipn)_4(H_2O)_2]^{4+}$, and hexafluorophosphate anions (Figure 6). The heterotetranuclear cations exhibit an overall ^{4}R rack-type architecture which is configurationally identical to that observed for the homotetranuclear cations in **5**. The two $[Cu(dipn)]^{2+}$ and the two $[Ni(dipn)(H_2O)]^{2+}$ subunits (*mer* isomers) are connected by the tetrakis(bidentate) ppba ligand in an *anti* planar conformation to give a centrosymmetric bis-binuclear entity (Figure 6a). The torsion angle around the N(amide)−C(phenylene) bond (ϕ) is 1.2(10)°, a value which is closer to 0° than that of **5** [ϕ = 12.7(7)°]. The intradimer copper−nickel distance (d) through the oxamato bridge is 5.503(1) Å, whereas the interdimer copper−copper distance (d') through the *para*-phenylenediamidato bridge is 8.4219(17) Å.

The copper atom exhibits a square-pyramidal geometry, CuN_4O, whereas the nickel atom has a distorted octahedral geometry, NiN_3O_3. The oxamato groups from the ppba ligand coordinate to the copper atoms through the amidate-nitrogen and the carboxylate-oxygen atoms, and they coordinate to the nickel atoms through the two carbonyl-oxygen atoms (Figure 6a). The copper basal plane is formed by three amine-nitrogen atoms of the dipn

ligand in a *mer* conformation [Cu−N = 2.024(6)−2.035(7) Å] and an amidate-nitrogen atom from the oxamato group of the bridging ppba ligand [Cu−N = 2.025(5) Å], while the axial position is occupied by a carboxylate-oxygen atom [Cu−O = 2.155(5) Å]. The nickel basal plane is formed by three amine-nitrogen atoms of the dipn ligand in a mer conformation [Ni−N = 2.068(5)−2.088(5) Å] and a carbonyl-oxygen atom from the oxamato group of the bridging ppba ligand [Ni−O = 2.116(4) Å], while the two axial positions are occupied by the other carbonyl-oxygen atom [Ni−O = 2.087(3) Å] and a water molecule [Ni−Ow = 2.121(5) Å]. As in **5**, the basal planes of the metal atoms are almost perpendicular to the plane of the oxamato group [ψ = 81.60(16) and 86.45(17)° for Cu(1) and Ni(1), respectively], and they are also disposed on opposite sides of the oxamato group (Figure 6b).

The four hexafluorophoshate anions are either weakly coordinated to the copper atoms [Cu(1)−F(7) = 3.776(8) Å] or hydrogen-bonded to the axially coordinated water molecules of the nickel atoms [O(1w)−F(12) = 2.933(8) Å] (Figure 6c). More importantly, the heterotetranuclear cations are connected through hydrogen bonds between the coordinated water molecules and the carbonyl-oxygen atoms from the oxamato groups [O(1w)−O(2) = 2.822(7) Å] leading to chains along the *c* axis (Figure 6c). The value of the intermolecular nickel−nickel distance between the two neighboring $Cu_2^{II}Ni_2^{II}$ entities is 5.4329(14) Å. In the crystal lattice, both the weakly coordinated and hydrogen-bonded PF_6^- anions occupy the small pores that result from the packing of these chains of $Cu_2^{II}Ni_2^{II}$ entities along the *a* axis (Figure S6, Supporting Information).

Magnetic Properties. The magnetic properties of **1**−**5** in the form of χ_M and $\chi_M T$ versus T plots, χ_M being the magnetic susceptibility per tetranuclear unit and T the temperature, are characteristic of either strong (**1**−**3**) or moderate (**4**) to weak (**5**) antiferromagnetically coupled Cu_4^{II} complexes (Figure 7). At room temperature, $\chi_M T$ varies in the range of 0.77−0.87 cm^3 K mol^{-1} for **1**−**3**, while it is equal to 1.35 and 1.61 cm^3 K mol^{-1} for **4** and **5**, respectively, values which can be compared with that expected for four magnetically isolated Cu^{II} ions ($\chi_M T$ = 1.65 cm^3 K mol^{-1} with g_{Cu} = 2.1). Upon cooling, $\chi_M T$ decreases continuously for **1**−**4** and it vanishes around 80 (**1**−**3**) and 15 (**4**) K (Figure 7a), while χ_M shows rounded maxima at 310 (**1**), 295 (**2** and **3**), and 70 (**4**) K (Figure 7b), suggesting thus a global antiferromagnetic intramolecular interaction with a singlet (S = 0) ground spin state. In contrast, $\chi_M T$ remains constant until 150 K for **5**, and then it decreases abruptly to reach a $\chi_M T$ value of 0.22 cm^3 K mol^{-1} at 2.0 K (Figure 7a). Indeed, χ_M shows a maximum at for **5** 3.0 K, which is characteristic of an S = 0 ground state (Figure 7b).

The temperature dependence of the magnetic susceptibility data of the homotetranuclear copper(II) complexes **1**−**5** were analyzed through the spin Hamiltonian for a "dimer-of-dimers" model (eq 1, with $S_1 = S_2 = S_3 = S_4 = S_{Cu} = 1/2$):

$$\mathbf{H} = -J(\mathbf{S}_1\cdot\mathbf{S}_2 + \mathbf{S}_3\cdot\mathbf{S}_4) - J'(\mathbf{S}_1\cdot\mathbf{S}_3) + g\beta(\mathbf{S}_1 + \mathbf{S}_3)B + g'\beta(\mathbf{S}_2 + \mathbf{S}_4)B \quad (1)$$

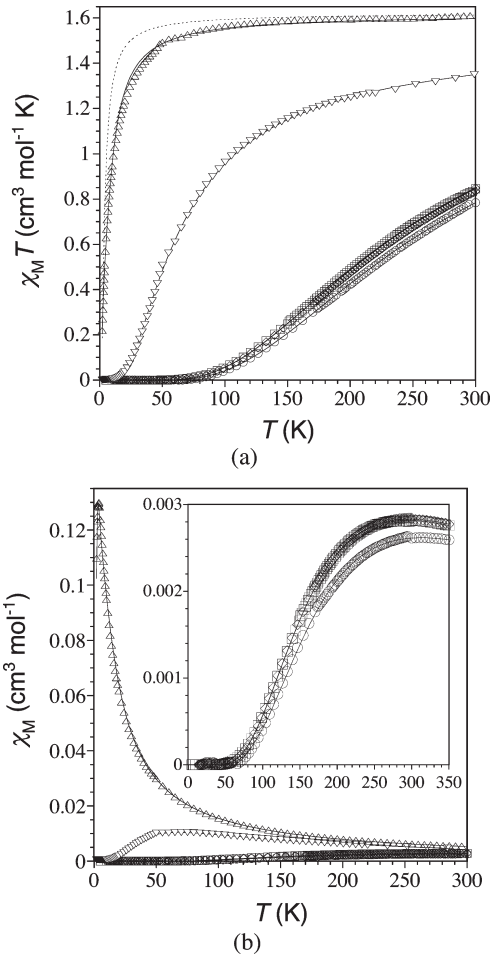

Figure 7. Temperature dependence of $\chi_M T$ (a) and χ_M (b) for **1** (○), **2** (□), **3** (◇), **4** (▽), and **5** (Δ). The inset shows the temperature dependence of χ_M for **1**−**3**. The solid and dotted lines are the best fit curves (see text).

where J ($J = J_{12} = J_{34}$) and J' ($J = J_{13}$) are the intra- and interdimer coupling constants between the Cu^{II} ions through the oxamato and phenylenediamidato bridges, respectively, and g and g' are the Zeeman factors of the Cu^{II} ions ($g = g' = g_{Cu}$).[17] The quality of the fit for **1**−**4** does not depend on the sign and magnitude of J', which can be varied from zero to a few tenths of cm^{-1}, either positive or negative, with a relatively small variation in the value of J. This fact suggests that, for **1**−**4**, the interdimer magnetic coupling through either the *meta*- or *para*-phenylenediamidato bridge is negligible compared to the intradimer one across the oxamato bridge. A least-squares fit of the experimental data through the Bleaney−Bowers equation for a dimer model gave J = −350(5) cm^{-1}, g = 2.09(1), and $R = 3.4 \times 10^{-4}$ for **1**; J = −330(5) cm^{-1}, g = 2.10(1), and $R = 3.0 \times 10^{-4}$ for **2**; J = −330(5) cm^{-1}, g = 2.10(1), and $R = 2.7 \times 10^{-4}$ for **3**; and J = −87.1(3) cm^{-1}, g = 2.03(1), and $R = 0.8 \times 10^{-4}$ for **4** (R is the agreement factor defined as $R = \sum[(\chi_M T)_{exp} - (\chi_M T)_{calcd}]^2/\sum[(\chi_M T)_{exp}]^2$. The theoretical curves reproduce very well the experimental data over the whole temperature range (solid lines in Figure 7). On the contrary, no satisfactory fit was obtained for **5** through a dimer model (with J' = 0), suggesting thus that the

(17) Ruiz, R.; Lloret, F.; Julve, M.; Faus, J.; Muñoz, M. C.; Solans, X. *Inorg. Chim. Acta* **1998**, *268*, 263.

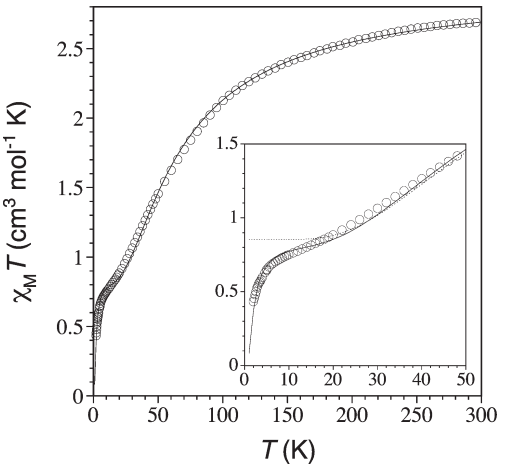

Figure 8. Temperature dependence of $\chi_M T$ for **6** (○). The inset shows the temperature dependence of $\chi_M T$ in the low-temperature region. The solid and dotted lines are the best fit curves (see text).

interdimer magnetic coupling through the *para*-phenylenediamidato bridge cannot be neglected as compared to the intradimer one across the oxamato bridge. A least-squares fit of the experimental data through the appropriate analytical expression[17] for a "dimer-of-dimers" model gave $J = -4.8(2)$ cm^{-1}, $J' = -14(1)$ cm^{-1}, $g = 2.08(1)$, and $R = 1.8 \times 10^{-4}$ for **5**. Indeed, the theoretical curve reproduces very well the experimental data over the whole temperature range when compared to that corresponding to two magnetically isolated dimers ($J' = 0$) (solid and dotted lines, respectively, in Figure 7).

On the other hand, the magnetic properties of **6** in the form of a $\chi_M T$ versus T plot, χ_M being the magnetic susceptibility per tetranuclear unit, are characteristic of a moderate antiferromagnetically coupled $Cu^{II}_2Ni^{II}_2$ complex (Figure 8). At room temperature, $\chi_M T$ is equal to 2.69 cm^3 K mol^{-1}, a value which is somewhat below that expected for the sum of two Cu^{II} ions ($\chi_M T = 0.83$ cm^3 K mol^{-1} with $g_{Cu} = 2.1$) and two Ni^{II} ions ($\chi_M T = 2.20$ cm^3 K mol^{-1} with $g_{Ni} = 2.1$) magnetically isolated. Upon cooling, $\chi_M T$ continuously decreases to reach a sort of plateau around 10 K with a $\chi_M T$ value of 0.75 cm^3 K mol^{-1}, and then it further decreases down to 0.43 cm^3 K mol^{-1} at 2.0 K (inset of Figure 8). This behavior indicates a global antiferromagnetic coupling with a singlet ($S = 0$) ground spin state. The temperature dependence of the magnetic susceptibility data of the heterotetranuclear copper(II)−nickel(II) complex **6** was analyzed through a spin Hamiltonian for a "dimer-of-dimers" model (eq 1, with $S_1 = S_3 = S_{Cu} = 1/2$ and $S_2 = S_4 = S_{Ni} = 1$), where g and g' are the Zeeman factors of the Cu^{II} and Ni^{II} ions, respectively ($g = g_{Cu}$ and $g' = g_{Ni}$). A least-squares fit of the experimental data by full-matrix diagonalization[18] gave $J = -50(1)$ cm^{-1}, $J' = -23(1)$ cm^{-1}, $g = 2.00(1)$, $g' = 2.11(1)$, and $R = 1.4 \times 10^{-4}$ for **6**. The theoretical curve reproduces very well the experimental data over the whole temperature range (solid line in Figure 8) when compared to that corresponding to two magnetically isolated dimers ($J' = 0$), which predicts a plateau at low temperatures where only the doublet states of each $S = 1/2$ $Cu^{II}Ni^{II}$ unit are thermally populated (dotted line in Figure 8).

(18) Cano, J. *VPMAG*; University of Valencia: Valencia, Spain, **2001**.

Table 8. Selected Magneto-Structural Data for **1**−**6**[a]

	J^a (cm^{-1})	J'^a (cm^{-1})	d^b (Å)	d'^b (Å)	ψ^c (deg)	ϕ^d (deg)
1	−350 (5)		5.190(2)	7.762(2)	3.8(2), 17.7(2)	91.0(3), 108.8(4)
2	−330(5)		5.224(2)	7.571(2)	6.7(2), 11.2(2)	90.7(5), 112.7(6)
3	−330(5)		5.185(2)	8.319(4)	5.4(2), 9.3(2)	98(2), 99(2)
4	−87.1(3)		5.491(1)	6.959(1)	89.0(2), 84.8(2)	82.1(1)
5	−4.8(2)	−14(1)	5.504(1)	8.454(1)	82.2(1), 86.1(1)	12.7(7)
6	−50(1)	−23(1)	5.503(1)	8.422(2)	81.6(2), 86.5(2)	1.2(10)

[a] J and J' are the magnetic coupling constants through the oxamato and phenylenediamidato bridges, respectively [$\mathbf{H} = -J(\mathbf{S}_1 \cdot \mathbf{S}_2 + \mathbf{S}_3 \cdot \mathbf{S}_4) - J'(\mathbf{S}_1 \cdot \mathbf{S}_3)$]. [b] d and d' are the metal−metal distances through the oxamato and phenylenediamidato bridges, respectively. [c] ψ is the dihedral angle between the metal basal planes and the oxamato plane. [d] ϕ is the torsion angle around the N(amide)−C(phenylene) bond.

Scheme 1. Exchange Coupling Orbital Pathways for the Oxamato-Bridged $Cu^{II}M^{II}$ (M = Cu and Ni) Dinuclear Fragments

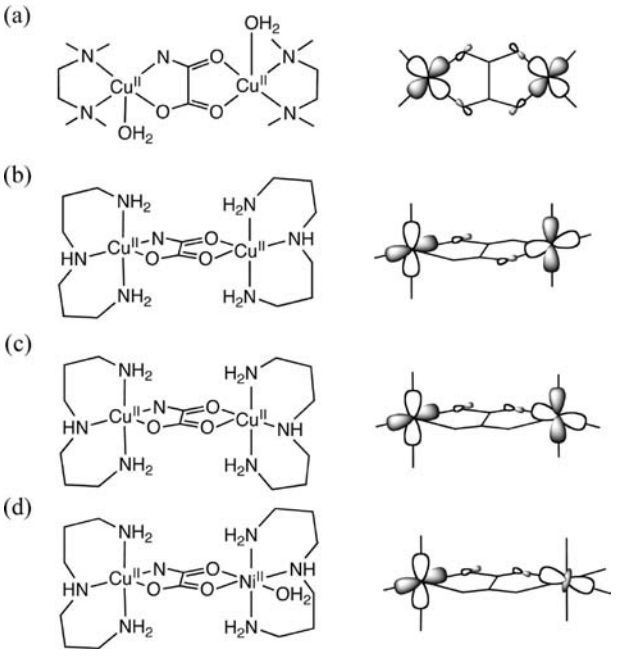

Selected magneto-structural data for this series of homo- and heterotetranuclear $Cu^{II}_2M^{II}_2$ rack compounds (M = Cu and Ni) with aromatic phenylenedioxamates as bridging ligands (L = mpba and ppba) and aliphatic di- and triamines as terminal ligands (L′ = Me_4en and dipn) are summarized in Table 8. The Cu^{II}_4 complexes exhibit either strong ($-J = 330-350$ cm^{-1}) or weak to moderate ($-J = 4.8-87.1$ cm^{-1}) antiferromagnetic intradimer coupling through the oxamato bridge depending on the bi-(**1**−**3**) or tridentate (**4** and **5**) nature of the terminal ligand, respectively. The calculated $-J$ values for **1**−**3** agree with those reported for related strong antiferromagnetically coupled oxamato-bridged dinuclear copper(II) complexes with bidentate terminal ligands ($-J = 366-425$ cm^{-1}).[19] The observed trend in the magnitude of the antiferromagnetic intradimer coupling for **1**−**5** is as expected when the bidentate ligand Me_4en is substituted by the tridentate ligand dipn, whereby the d_{xy}(Cu)-type magnetic orbitals centered on each Cu^{II} ion are either

(19) (a) Verdaguer, M.; Kahn, O.; Julve, M.; Gleizes, A. *Nouv. J. Chim.* **1985**, *9*, 325. (b) Emori, S.; Todoko, K. *Bull. Chem. Soc. Jpn.* **1993**, *66*, 3513.

coplanar [$\psi = 3.8-17.7°$ for **1**−**3**] or noncoplanar [$\psi = 82.2-89.0°$ for **4** and **5**] with the oxamato bridge, respectively (Scheme 1a−c). The $Cu^{II}_2Ni^{II}_2$ complex with a tridentate terminal ligand (**6**) shows a moderate antiferromagnetic intradimer coupling ($-J = 50$ cm^{-1}). The calculated $-J$ value for **6** is somewhat smaller than those reported for related oxamato-bridged dinuclear copper(II)−nickel(II) complexes ($-J = 104.2-108.0$ cm^{-1}).[20] This situation is as expected when the Cu^{II} ion is replaced with the Ni^{II} one, whereby the additional d_{z^2}(Ni)-type magnetic orbital is coplanar with the oxamato bridge but not the d_{xy}(Cu)-type magnetic orbital [$\psi = 84.8°$ for **6**] (Scheme 1d).

As a matter of fact, the coupling constant (J) for metal ions with more than one unpaired electron can be decomposed into a sum of individual exchange coupling contributions (J_{ij}) involving each pair of magnetic orbitals according to $J = (1/n_A n_B)\sum_{i,j} J_{ij}$, where $i = 1 - n_A$ and $j = 1 - n_B$.[21] Hence, the magnitude of the intradimer antiferromagnetic coupling along this series of $Cu^{II}_2M^{II}_2$ complexes is not properly described by J but by $n_A n_B J$ (with $n_A = n_B = 1$ for M = Cu^{II} and $n_A = 1$ and $n_B = 2$ for M = Ni^{II}), which depends on the nature and magnitude of each pairwise contribution according to $J = J_{xy,xy}$ (M = Cu^{II}) and $2J = J_{xy,xy} + J_{xy,z^2}$ (M = Ni^{II}). On the basis of the simple orbital model elaborated by Kahn and co-workers, the absolute value of J_{ij} is proportional to the square of the overlap integral S_{ij} ($|J_{ij}| \alpha S_{ij}^2$).[21] So, complexes **1**−**3** present the strongest antiferromagnetic interaction between the Cu^{II} ions ($-J = 330-350$ cm^{-1}) due to the coplanar disposition of the two d_{xy}(Cu)-type magnetic orbitals, a situation which maximizes the overlap (s) between the p_y and p_y nitrogen or oxygen orbitals along each side of the oxamato bridge ($|J_{xy,xy}| \alpha 4s^2$ with $S_{xy,xy} = 2s$) (Scheme 1a). Complex **5** shows instead the weakest antiferromagnetic interaction ($-J = 4.8$ cm^{-1}) because of the noncoplanar disposition of the d_{xy}(Cu)-type magnetic orbitals, a situation which minimizes the orbital overlap (s) along each side of the oxamato bridge ($|J_{xy,xy}| \approx 0$ with $S_{xy,xy} = 0$; Scheme 1b). For **4**, however, the antiferromagnetic interaction ($-J = 87.1$ cm^{-1}) is 4 times weaker than that for **1**−**3** ($-J = 330-350$ cm^{-1}), in perfect agreement with that expected for a side-by-side orientation of the d_{xy}(Cu)-type magnetic orbitals in a noncoplanar disposition, which makes either maximum or minimum the orbital overlap (s) along each side of the oxamato bridge ($|J_{xy,xy}| \alpha s^2$ with $S_{xy,xy} = s$; Scheme 1c). A similar situation is found for complex **6**, where the overall antiferromagnetic interaction given by $2J$ is close to that of **4** in reasonable agreement with that expected for a side-by-side orientation of the d_{z^2}(Ni)- and d_{xy}(Cu)-type magnetic orbitals in a mixed coplanar/noncoplanar disposition, which also makes either maximum or minimum the individual orbital overlap (s) along each side of the oxamato bridge ($|J_{xy,z^2}| \alpha s^2$ with $S_{xy,z^2} = s$; Scheme 1d).

Unfortunately, the ferro- or antiferromagnetic nature and the overall magnitude of the interdimer coupling between the Cu^{II} ions through the aromatic phenylene spacer cannot be determined unambiguously for the Cu^{II}_4 complexes with the *meta*-phenylenedioxamato bridging ligand (L = mpba) and the terminal bi- and tridentate ligands, Me_4en (**1** and **2**) and dipn (**4**), respectively, because of the much stronger antiferromagnetic intradimer coupling through the oxamato bridges. In this respect, it must be noticed that a related dinuclear copper(II) complex with double *m*-phenylenediamidato bridges shows a moderate ferromagnetic coupling ($J' = +16.8$ cm^{-1}).[11a] The same situation holds for the Cu^{II}_4 complex with the *para*-phenylenedioxamato bridging ligand (L = ppba) and the terminal bidentate Me_4en ligand (**3**). Yet, for the $Cu^{II}_2M^{II}_2$ complexes (M = Cu and Ni) with the *para*-phenylenedioxamato bridging ligand (L = ppba) and the terminal tridentate dipn ligand (**5** and **6**), a moderate antiferromagnetic interdimer coupling ($-J' = 14-23$ cm^{-1}) has been observed across the aromatic phenylene spacer with a *para*-substitution pattern. The calculated $-J'$ values for **5** and **6** contrast with those earlier reported for related dinuclear copper(II) complexes with double *p*-phenylenediamidato bridges, which show a moderate to strong antiferromagnetic coupling ($-J' = 81-95$ cm^{-1}).[11b] This situation agrees with the occurrence of a σ-type orbital pathway through the bridging ppba ligand in a planar conformation for **5** and **6** ($\phi = 1.2-12.7°$), instead of the π-type orbital pathway that would be operative for a nonplanar but orthogonal conformation of the bridging mpba and ppba ligands for **1**−**4** ($\phi = 82.1-112.7°$; Scheme 2). In the

Scheme 2. Exchange Coupling Orbital Pathways for the Phenylenediamidato-Bridged Cu^{II}_2 Dinuclear Fragments

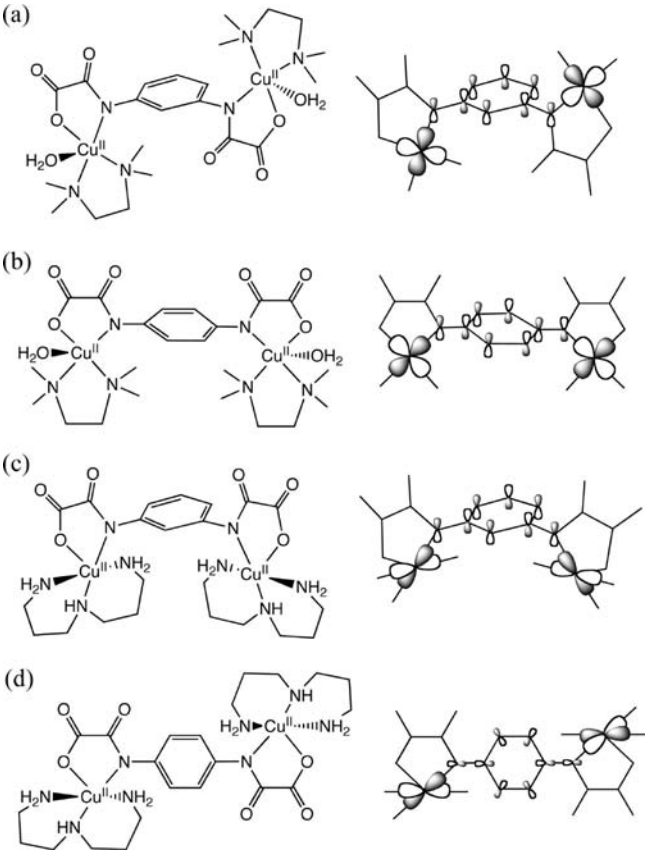

(20) (a) Gao, E. Q.; Tang, J. K.; Liao, D. Z.; Jiang, Z. H.; Yan, S. P.; Wang, G. L. *Inorg. Chem.* **2001**, *40*, 3134. (b) Tercero, J.; Díaz, C.; Ribas, J.; Solans, X.; Maestro, M.; Mahía, J.; Stoeckli-Evans, H. *Inorg. Chem.* **2003**, *42*, 3366.

(21) Kahn, O. *Molecular Magnetism*; VCH: New York, USA, **1993**.

former case, the d_{xy}(Cu)-type magnetic orbitals centered on each Cu^{II} ion are weakly delocalized onto the p_x and p_y nitrogen and carbon orbitals of the phenylenediamidate bridges (Scheme 2d), in such a way that the spin polarization effects are negligible. In contrast, they are largely delocalized onto the p_z nitrogen and carbon orbitals of the phenylenediamidato bridges in the latter case (Scheme 2a−c), a situation which maximizes the spin polarization effects. In fact, with some notable exceptions, the spin polarization mechanism requires a π-type orbital pathway to efficiently compete with the spin delocalization one.[22] So, the somewhat reduced but non-negligible antiferromagnetic interaction across the *p*-phenylenediamidato bridge for **5** and **6** in spite of the long metal−metal distances (d' = 8.42−8.45 Å) can be explained by the relatively small metal−ligand orbital mixing. The weaker antiferromagnetic interaction for **5** ($-J'$ = 14 cm^{-1}) as compared to that for **6** ($-J'$ = 23 cm^{-1}) is thus explained by the larger deviations from planarity (ϕ = 12.7 and 1.2°, respectively), as expected for σ-type orbital pathways.

Conclusion

In this work, homo- and heterotetranuclear copper(II) and copper(II)−nickel(II) rack compounds with aromatic *meta*- and *para*-substituted phenylenedioxamates as bridging ligands (L = mpba and ppba) and aliphatic di- and triamines as terminal ligands (L′ = Me_4en and dipn) have been rationally prepared by following a molecular-programmed self-assembly method. The nature of the bridging ligand (*meta*- or *para*-substitution pattern of the aromatic spacer) as well as the terminal ligand (di- or tridentante character) have a strong influence on their molecular structures and magnetic properties. Let us briefly recall the main results on each point from a ligand design perspective:

(i) From a structural point of view, the heterotopic nature of the bridging mpba and ppba ligands allows the preparation of both homo- and heterometallic racks owing to the presence of two different bidentate O,O- and N,O-oxamato donor groups. This situation contrasts with the vast majority of previously reported homometallic racks prepared from homotopic bridging ligands. Moreover, because of their rotational freedom around the C−N bond, they can adopt either a planar or a nonplanar conformation in their metal complexes mainly depending on the geometric constraints of the terminal ligands. So, because of the steric hindrance with the "in-plane" bidentate terminal ligand Me_4en, the bridging mpba and ppba ligands present a noncoplanar conformation, with the two oxamato groups tilted up or down with respect to the plane of the phenylene spacer. In the absence of steric hindrances, the bridging mpba and ppba ligands can adopt either a noncoplanar or a planar conformation depending on the side-by-side or opposite-side disposition, respectively, of the "out-of-plane" tridentate terminal ligand dipn.

(ii) From a magnetic point of view, the bridging mpba and ppba ligands combine the well-known efficiency of the oxamato bridge, $C_2O_3NR^{2-}$, to transmit the magnetic coupling in oxamato-bridged dicopper(II) complexes, together with the less-studied magnetic coupling through extended π-conjugated aromatic bridges, $C_6H_4(NR)_2^{2-}$, in phenylenediamidato-bridged dicopper(II) complexes. Thus, the antiferromagnetic coupling across the oxamato bridge dramatically decreases when replacing the in-plane bidentate Me_4en ligand with the out-of-plane tridentate dipn ligand because of the poorer orbital overlap through the σ-type orbital pathway of the oxamato bridge. Similarly, the antiferromagnetic coupling across the *p*-phenylene spacer decreases in the planar bridging ppba ligand. This situation agrees with the occurrence of a σ-type orbital pathway (spin delocalization mechanism) instead of the π-type orbital pathway that would be operative for a nonplanar but orthogonal conformation of the aromatic bridging ligand (spin polarization mechanism).

Acknowledgment. This work was supported by the MEC (Spain) (Projects CTQU2007-61690, MAT2007-60660, and "Factoria de Crystalización, CSD2006-00015 CONSOLIDER INGENIO-2010"), the CNRS (France) and the CAPES (Brazil). E.P. and D.C. thank the MEC and the CAPES for grants.

Supporting Information Available: Crystal packing views of **1**−**6** (Figures S1−S6). This material is available free of charge via the Internet at http://pubs.acs.org. Crystallographic data (excluding structure factors) for the structures reported in this paper have been deposited with the Cambridge Crystallographic Data Centre as supplementary publication numbers CCDC-650175 (**1**), CCDC-650176 (**2**), CCDC-711356 (**3**), CCDC-711357 (**4**), CCDC-711358 (**5**), and CCDC-711359 (**6**). Copies of the data can be obtained free of charge on application to CCDC, 12 Union Road, Cambridge CB21EZ, UK (fax: (+44) 1223 336 033; e-mail: deposit@ccdc.cam.ac.uk).

(22) (a) Glaser, T.; Gerenkamp, M.; Fröhlich, R. *Angew. Chem., Int. Ed.* **2002**, *41*, 3823. (b) Glaser, T.; Heidemeier, M.; Strautmann, J. B. H.; Bögge, H.; Stammler, A.; Krickemeyer, E.; Huenerbein, R.; Grimme, S.; Bothe, E.; Bill, E. *Chem.—Eur. J.* **2007**, *13*, 9191.